JOURNAL OF MATERIALS SCIENCE 26 (1991) 5547–5560

Ceramic composites: TiB_2–TiC–SiC

Part I *Properties and microstructures in the ternary system*

F. de MESTRAL, F. THEVENOT
Ecole Nationale Supérieure des Mines de Saint-Etienne, 158 cours Fauriel, 42023 St. Etienne Cedex, France

In the ternary system TiB_2–TiC–SiC, the different two-phase composites, TiC–TiB_2, SiC–TiB_2 and SiC–TiC exhibit remarkable mechanical properties in regard with the single phase ceramics. The evolution of those properties, i.e. modulus of rupture σ_f, fracture toughness K_{1c}, critical flaw size a_c, hardness Hv, coefficient of thermal expansion α and electrical resistivity ρ, over the complete ternary diagram was investigated.

A methodology of research using optimal design was used to minimize the number of composites to be elaborated. In this study, 16 samples were sufficient to empirically determine a provisional mathematical model for each property. A model, then, enables the plot of isoresponse curves in the ternary diagram. The samples were hot pressed and the optimal hot-pressing cycles were determined using densification rates against temperature curves. The concordance between computed and experimental values is excellent, e.g. a sample containing 20 mol% of TiB_2, 55 mol% of TiC and 25 mol% of SiC has $\sigma_{fexp} = 1080$ MPa, $\sigma_{fcomp} = 1070$ MPa; $K_{1cexp} = 6.7$ MPa $m^{1/2}$, $K_{1ccomp} = 6$ MPa $m^{1/2}$; $Hv_{exp} = 16.6$ GPa, $Hv_{comp} = 17.3$ GPa; and $\rho_{exp} = 57.4$ $\mu\Omega$ cm, $\rho_{comp} = 55$ $\mu\Omega$ cm.

Although titanium diboride does not react with silicon carbide, a strong interface bond is developed between titanium diboride and titanium carbide, and between titanium carbide and silicon carbide. This explains the bend strength evolution in the ternary system, and more particularly the fact that, in the area $\sigma_f > 1000$ MPa and $K_{1c} > 6$ MPa $m^{1/2}$, to high SiC contents correspond to low TiB_2 contents and conversely. The relevant microstructures will be discussed.

1. Introduction

Carbide and boride ceramics have intrinsic characteristics, i.e. high melting point, high hardness, good chemical inertness, high wear resistance, good strength, that make them suitable candidates for thermomechanical applications. However, the use of those single phase ceramics, even fully densified, in structural or wear applications is limited by the variability of their mechanical strength and their poor fracture toughness. The scatter of the strength measurements is usually attributed to microstructural defects such as pores, inclusions, exaggerated grain growth or nonuniform sintering. The number of those defects, and hence their influence, could be seriously reduced by a careful mastery of each step of the elaboration process.

Second phase additions can improve the strength and the fracture toughness of single phase ceramics. This second phase can act as a particle phase transforming toughening, e.g. zirconia toughened alumina, or as an intergranular binder, either glassy, e.g. SIALONs, or metallic, e.g. WC–Co. Although these methods are quite efficient at room temperature, the toughening mechanisms do not hold with increasing temperatures. This is due either to inappropriate phase transformation, or to binder softening or recrystallization. However, the use of a second phase that is both thermodynamically and chemically stable with the host matrix will allow the retention of the matrix-second phase intrinsic properties, even at elevated temperatures. Depending on the physical characteristics and the shape of the second discrete phase, i.e. fibres, whiskers or particles, the toughening mechanisms can be fibres pullout or shearing, crack tip deflection or pinning, and/or crack tip stress redistribution.

The good electrical conductivity of titanium diboride as well as its chemical inertness at high temperatures make it a good candidate for special electrical applications [1], e.g. cathodes used in aluminium electrosmelting or vapourizing elements for vacuum metal deposition installations. However these applications are mainly limited by TiB_2 poor fracture toughness and its sensitivity to slow subcritical crack growth. Titanium carbide was found to be an efficient toughening second phase [1, 2].

High density silicon carbide is an extremely hard and wear resistant material which has, furthermore, excellent corrosion, thermal shock and oxidation resistance. All these properties together with its good high temperature strength allow the use of SiC for numerous structural and wear applications, e.g. heat exchanger, metal working parts, nozzles . . . However, once more, SiC moderate fracture toughness limits its use under severe conditions. Additions of TiB_2 [3, 4,

0022–2461/91 $03.00 + .12

5] or TiC [5–7] particles were found to be effective in terms of increasing fracture toughness. Titanium carbide has a further advantage since it possesses five independent slip systems which allow the material to be ductile above $\approx 800\,^{\circ}C$ [8]. Such plasticity may result in a stress redistribution at the crack tip and, hence, toughens the composite at high temperatures.

Composites based on the three ceramics, TiB_2–TiC–SiC, could be tailored with very different characteristics, depending on which phase is the major constituent. A predominance of SiC would lead to a composite for structural and corrosion applications, and a composite based on TiC or TiB_2 could be used for electrical applications. The knowledge of the composites properties for every composition over the complete ternary diagram would be paramount for the selection of an optimized composite for a determined application. The present paper discusses the evolution of properties in the complete ternary system: modulus of rupture σ_f, fracture toughness K_{1c}, critical flaw size a_c, hardness Hv, coefficient of thermal expansion α (CTE) and electrical resistivity ρ.

2. Methodology

It has been shown that the different two-phase composites TiB_2–TiC, SiC–TiB_2, SiC–TiC, exhibit much better mechanical properties than the single phase ceramic, TiB_2, TiC and SiC [1, 3, 6]. Would the addition of the third phase in the composites further improve those mechanical characteristics? One classical way of answering this question could be to take a well-known two-phase ceramic, e.g. SiC–TiB_2, and study the effect of the substitution of some TiB_2 by TiC. Although this technique may lead to good results, it does not allow to find the optimum composition of the ternary system. This last point would require the knowledge of a property value for an infinite number of compositions, which is obviously non-applicable. Even if the study is limited to compositions taken every 10 or 5 per cents, it would require the manufacture of 66 and, respectively, 231 samples, which is still prohibitive. A methodology of research using a statistical approach is hence necessary.

Phan-Tan-Luu developed a methodology of research using optimal design [9, 10] and applied it to the problems of mixtures [11, 12]. The aim of the methodology consists in describing, predicting or explaining the studied phenomenon, i.e. finding the relations between the factors (in this study, the composition of the composites) and the responses (here, the different properties). This is done with a limited number of points by substituting the local knowledge by a space knowledge using mathematical models.

In this study, polynomial models up to the third degree were developed. The time required to optimize the complete processing route of every composite was estimated to be prohibitive. Therefore, the arbitrary choice was made, first to determine the best composition on non-optimized samples and, only then to optimize its whole elaboration process. However, the validity of a composite for its use in the model's calculation still has to be assessed. Two criteria are used: density and microstructure. The density has to be higher than 98% of theoretical density (computed using the mixture rule) and a visual check has to make sure the microstructure is fine and homogeneous.

3. Experimental procedures

The starting powders were: titanium diboride, grade A from Starck (Berlin), mean particle size $\approx 4\,\mu m$; titanium carbide ceramic grade C.A.S. from Starck, mean particle size $\approx 3\,\mu m$ and α silicon carbide from ESK (Germany) mean particle size $\approx 1\,\mu m$. The powders were desagglomerated in ethanol with an ultrasonic desintegrator, and then mixed for three days in a small ballmill. The mixture was vacuum dried and sieved at 200 μm. The powders were then hot-pressed in graphite dies under 40 MPa in argon atmosphere in tablets with 20 mm in diameter and 15 mm in height. The resulting ceramic cylinders were cut by electron discharge machining in four bars of dimensions $3 \times 4 \times 18\,mm^3$. One face of these bars was carefully polished down to 3 μm with diamond paste and its edges were beveled. The flexural strength was measured under 3 point bending (15 mm outer span), the fracture toughness was determined using the Vickers indentation technique (carried out at l'Ecole Nationale Supérieure des Mines de Paris), the coefficient of thermal expansion between 20 and 1200 °C under argon and the electrical resistivity was measured with the four linear points method.

3.1. Hot-pressing technique

The material used is a laboratory press, type VS Pgr 7/10 from Degussa [13, 14]. The temperature limit of the graphite resistor is 2500 °C. A double-action pneumatic jack can develop forces up to 20 kN. Since the inner diameter of the die is 20 mm, a pressure of 60 MPa can be reached. It is, however, limited to 40 MPa due to the graphite creep resistance. The working atmosphere is either vacuum or inert gas.

The special feature about this press is that, both the measure and the control of the temperature, pressure and displacement are completely computerized. This allows a very close control of the phenomenon occurring during sintering. The selected mixtures were hot-pressed a first time and the related densification rate versus temperature curves were plotted (Fig. 1). The overall dilatation of the system press plus carbon die and plungers was found to be linear from 800 to 2100 °C. Therefore, it is possible to neglect it since it will only influence the height of the densification rate peak but will not cause any shifting of its actual position.

From these plots, the optimum hot-pressing cycles were determined. A 0.5 h stage at the temperature of maximum densification rate was found to result in samples having approximately 95% theoretical density. A second stage about 150 °C above is necessary to achieve full densification. A typical hot-pressing cycle plot is given for a composite with 33.3 mol % of each phase (Fig. 2). It consists in a first stage at 1800 °C for

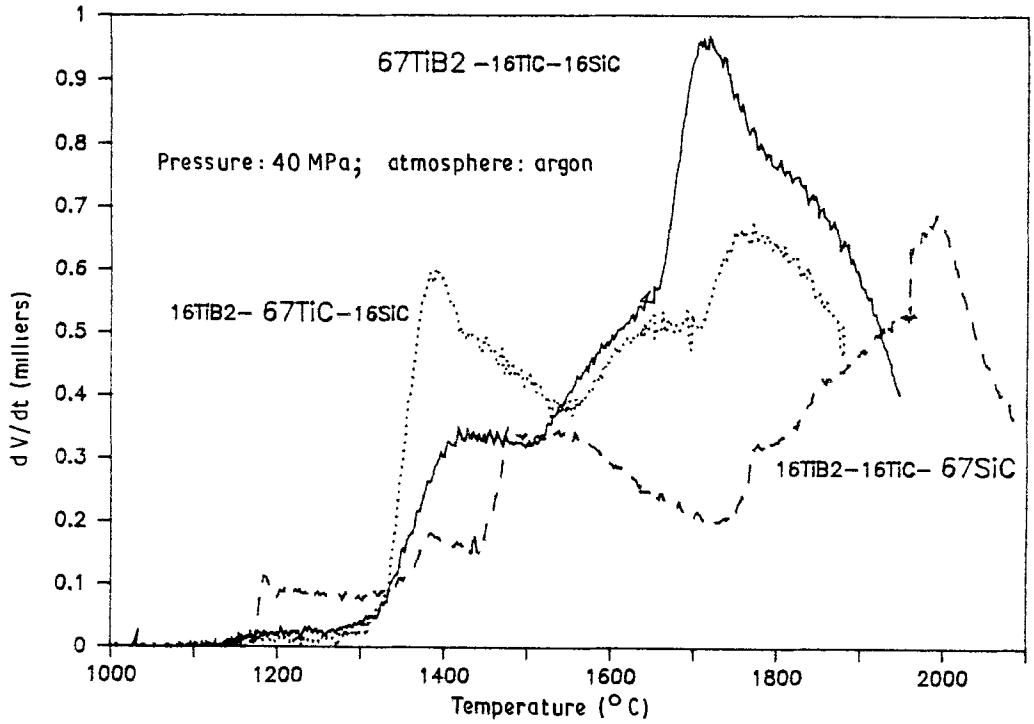

Figure 1 Densification rate against temperature curves for three different composites.

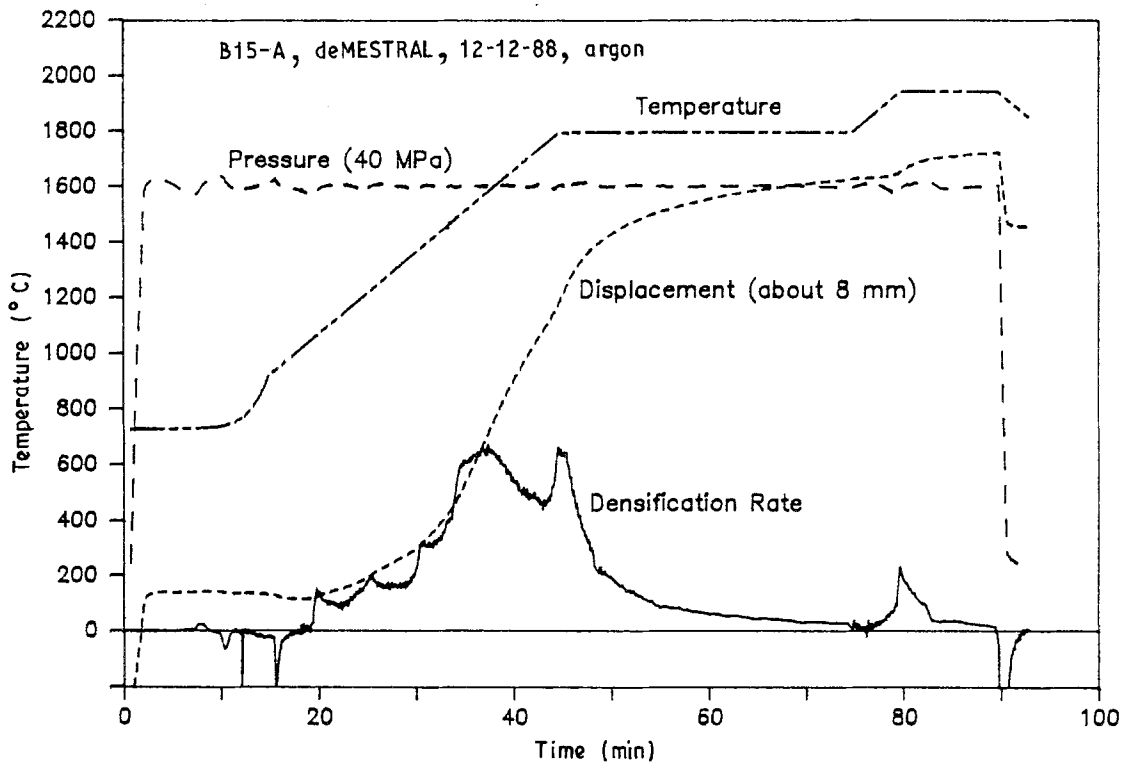

Figure 2 Typical hot-press control plot showing the temperature, the plungers displacement, the pressure and the densification rate as function of time.

30 min and a second one at 1950 °C for 10 min; the heating and cooling rates are of 30 °C min^{-1}; the applied pressure was 40 MPa. The advantage of such a cycle is that most of the densification occurs at a rather low temperature and that the higher temperature stage is short. Therefore, there is no time for grain growth to occur, and the resulting microstructure is fine and homogeneous.

4. Results and discussion

4.1. Interactions in the system

Dense cylinders of TiB_2, TiC and SiC, polished down to 6 μm, were held together at 2100 °C for 2 h under 40 MPa. The first evidence is that no reaction at all occurred between TiB_2 and SiC since the two tablets fall apart once pushed out of the die. This is consistent with the observations of McMurtry *et al.*, [3]. How-

ever, the two other diffusion couples were found to be firmly bonded. Fig. 3 shows the TiB_2–TiC interface. TiC diffused in TiB_2 on an average distance of 50 μm. Ordon'yan [15] found a very small solubility of TiB_2 in TiC at temperatures equal or higher than 2100 °C. Since both materials exhibit a very similar coefficient of thermal expansion (CTE) ($\approx 8\ 10^{-6}\ K^{-1}$), no interface stresses are generated during cooling. It is therefore possible to assume a very strong cohesion between TiB_2 and TiC particles.

The interface between TiC and SiC (Fig. 4) exhibits a marked degradation of the TiC region. This is due to the large CTE mismatch, i.e. $8 \times 10^{-6}\ K^{-1}$ for TiC and $4.8 \times 10^{-6}\ K^{-1}$ for SiC. However, this degradation proves that both materials develop very strong bonds even at 2100 °C. Wei and Becher [6] also concluded to strong TiC–SiC bonds since they found no evidence of interfacial debonding in their composite, and Jiang [16] proved it with a TEM study of a TiC–SiC composite. Diffusion takes place in SiC on an average distance of 20 μm (Fig. 4). This diffusion seems to be favoured by the presence of Fe and Co.

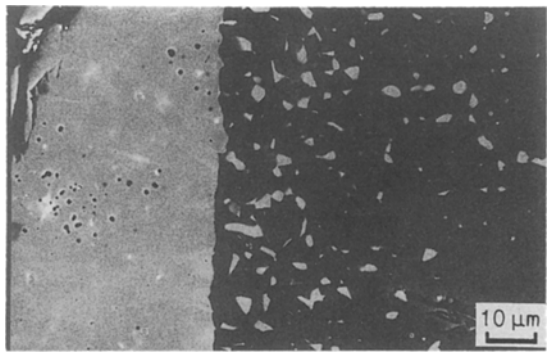

Figure 3 TiB_2 (black)–TiC (white) interface (2100 °C, 2 h, 40 MPa).

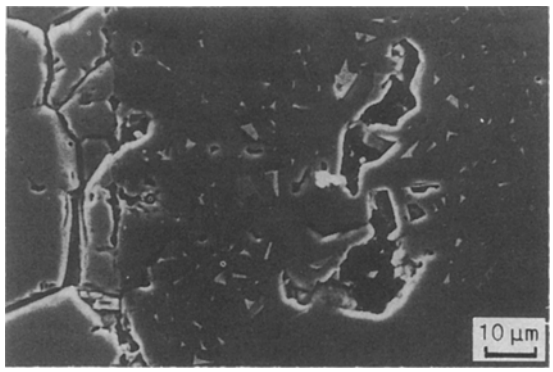

Figure 4 SiC (black)–TiC (white) interface (2100 °C, 2 h, 40 MPa).

4.2. Bend strength

The bend strength of eighteen different composites are listed in Table I. The flexural strength of pure TiC and pure SiC are rather low in regard of the values obtained for the other composites, i.e. 550 ± 10% MPa and 500 MPa, respectively. Of the three 50–50 % composites, it is normal for the TiB_2–SiC combination to exhibit the lower flexural strength (630 ± 7% MPa) since there is no or little interaction between SiC and TiB_2 particles. The other two-phase composites, TiC–TiB_2 and TiC–SiC, have satisfactory modulus of rupture, i.e. 950 ± 10% MPa and 910 ± 8 %, respectively. This is consistent with the interaction observations since TiC was found to develop strong bonds with both TiB_2 and SiC. It is interesting to notice that the higher flexural strengths ($\sigma_f > 1000$ MPa) are located in an area located "far away" from the TiB_2–SiC axis. The maximum SiC content of these compositions, i.e. point 8, 9, 12, 15 and 17, never gets over 33 mol %. The average standard deviation is around 10 %, and since we are dealing with strength up to nearly 1100 MPa, the precision of the mathematical model cannot be better than ± 100 MPa.

TABLE I Experimental values of flexural strength and their differences with polynomial models of first, second, reduced cubic and cubic degrees

	TiB_2 (mol %)	TiC	SiC	Flexural strength (MPa)	Differences with polynomial models of degree 1st	2nd	cub. red.	3rd
1	100	0	0	890 ± 24	84	23	20	13
2	0	100	0	550 ± 54	388	63	60	9
3	0	0	100	500	122	− 46	− 49	10
4	50	50	0	950 ± 98	6	84	88	90
5	50	0	50	628 ± 43	170	110	113	111
6	0	50	50	907 ± 70	− 127	45	48	48
7	33	33	33	970 ± 77	− 126	20	0	0
8	67	33	0	1030 ± 140	− 67	24	27	51
9	33	67	0	1083 ± 164	− 133	− 129	− 126	− 51
10	67	0	33	973 ± 75	− 117	− 165	− 162	− 63
11	33	0	67	624 ± 15	115	31	34	− 63
12	0	67	33	1040 ± 75	− 208	− 109	− 105	− 27
13	0	33	67	831 ± 130	− 104	48	51	− 27
					test points			
14	67	16.5	16.5	980 ± 107	− 70	− 3	− 12	5
15	16.5	67	16.5	1074 ± 24	− 183	− 127	− 136	− 17
16	16.5	16.5	67	716 ± 48	135	79	69	− 67
17	32	55	13	1073 ± 131	− 165	− 65	77	13
18	20	55	25	1075 ± 106	− 209	− 82	− 96	− 11

Therefore the validity criterion for a model is that both the polynomial fitting and the test points fall within 100 MPa of the experimental data.

The mathematical model developed for the description of a property being purely empirical, it has to remain as simple as possible. To illustrate this point, the difference between the theoretical values, computed with linear, quadratic, reduced cubic and cubic polynoms, and the experimental data are reported in Table I. The four models are determined using points 1 to 13. Since there are more points than theoretically necessary, a polynomial fitting is made (NEMROD [12]) which explains the discrepancy between the experimental measurements and calculated values. Points 14 to 18 are test points only used to assess the validity of the models. The first degree model is of really poor quality since both the polynomial fitting and the test points exhibit differences Δ with the measured values much higher than 100 MPa ($13\,\Delta > 100$ MPa and Δ max. = 388 MPa). The quadratic and the reduced cubic models are already more accurate since the regression generates four values with $\Delta > 100$ MPa (Δ max. = 165 MPa) and only one test point has a difference higher than 100 MPa. However it is still not satisfactory. On the other hand, with the complete cubic model only one point has $\Delta > 100$ MPa and the three test points 14, 15 and 16 have accurate predicted values. ($\Delta < 67$ MPa). It is therefore concluded that the cubic model (Equation 1) satisfactorily describes the evolution of the bend strength over the complete ternary diagram.

$$\begin{aligned} Y = {} & 903X_1 + 559X_2 + 510X_3 \\ & + 1238X_1X_2 + 133X_1X_3 + 1683X_2X_3 \\ & - 1132X_1X_2(X_1 - X_2) + 1472X_1X_3 \\ & \times (X_1 - X_3) + 1301X_2X_3(X_2 - X_3) \\ & - 714X_1X_2X_3 \end{aligned} \quad (1)$$

where Y is the flexural strength and X_i the molar fraction of i, with 1 : TiB_2, 2 : TiC, 3 : SiC.

Once the polynomial model is determined it is possible to plot isoresponse curves. Fig. 5 shows the predicted isoflexural strength curves in the complete ternary diagram. The experimental measurements are also reported to allow direct comparison with the predicted values.

This third degree polynomial model predicts a maximum bend strength value of 1087 MPa for the composition 32 mol % TiB_2, 55 mol % TiC, 13 mol % SiC. This is an obvious point to check to assess the validity of the model. The experimental strength is found to be $1073 \pm 12\%$ MPa (point 17). The correspondence between the experimental and the predicted values is excellent. A backscattered electron image of this optimum composite microstructure is

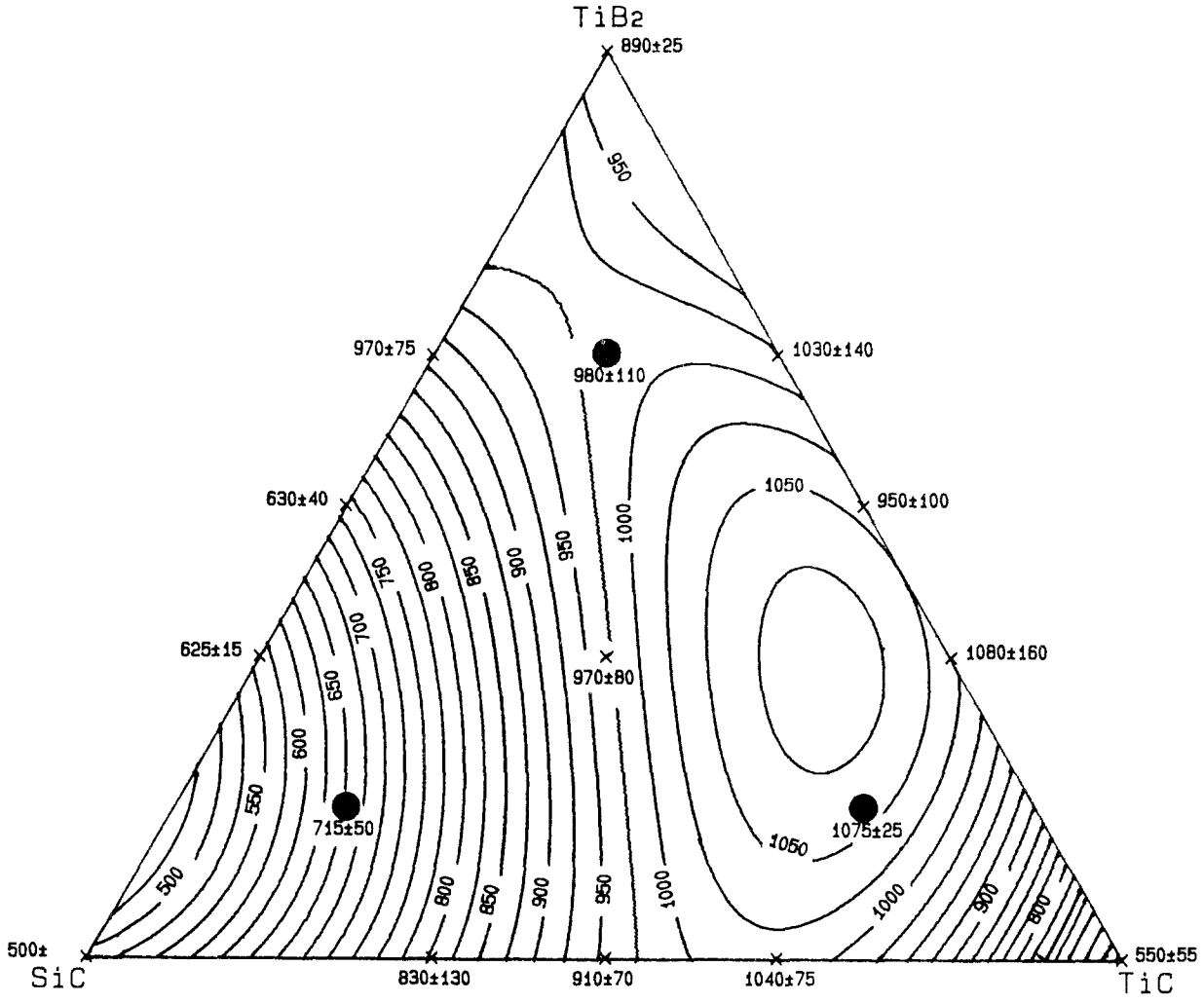

Figure 5 Isobend strength curves plotted using a third order polynomial model. The incrementation step between two curves is 25 MPa. The black points are test points.

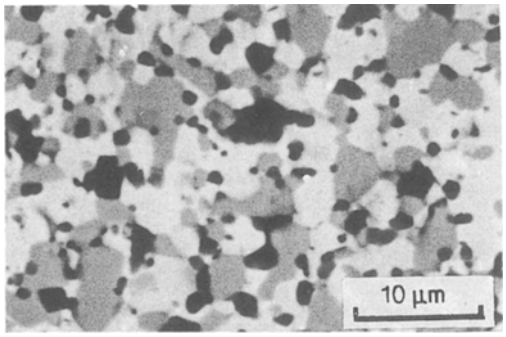

Figure 6 Backscattered electron micrograph of the maximum bend strength composite (No. 17), i.e. 32 mol % TiB_2 (grey)–55% TiC (white)–13% SiC (black).

given in Fig. 6. Nearly every grain of both discrete phases TiB_2 and SiC is surrounded by the TiC matrix. Therefore, the number of weak TiB_2–SiC contact points is of minor importance in regard with the strong TiC–SiC and TiC–TiB_2 interactions. This is consistent with the fact that, in the large area $\sigma_f > 1000$ MPa, to high SiC content corresponds low TiB_2 content and inversely, i.e. large SiC amounts are never found together with large TiB_2 amounts.

The flexural strength at 1200 °C for the three phase composites is determined under nitrogen (Table II). The sharp decrease is due to the degradation of the surface layer by nitrogen. TiC being the more sensitive, composite 15 and 18 exhibit the larger difference. On the other hand, for composite 16 (67 mol % SiC) only a slight decrease is measured (26%). This is due to the good inertness of SiC to nitrogen.

4.3. Fracture toughness

The fracture toughness of the single phase ceramics are relatively low, i.e. 5 MPa $m^{1/2}$ for TiB_2, 4.4 MPa $m^{1/2}$ for TiC and 2.9 MPa $m^{1/2}$ for SiC (see Table III). The two phase composites exhibit already a higher K_{1c}, i.e. 5.2 MPa $m^{1/2}$ for TiB_2–TiC, 6.3 MPa $m^{1/2}$ for SiC–TiC and 5.1 MPa $m^{1/2}$ for SiC–TiB_2. However, the best fracture toughness values were measured for the three phase composites, i.e. the four of them (points 7, 14, 15, and 16) have an average value of 6.1 ± 0.2 MPa $m^{1/2}$.

A second order polynomial model (Equation 2) is sufficient to describe the evolution of the fracture toughness over the complete ternary diagram.

$$Y = 5.1X_1 + 4.4X_2 + 3X_3 + 2.7X_1X_2 + 5.4X_1X_3 + 11.2X_2X_3 \quad (2)$$

where Y is the fracture toughness and X_i the molar fraction of i, with 1 : TiB_2, 2 : TiC, 3 : SiC.

The maximum difference between the predicted and the measured values is 0.7 MPa $m^{1/2}$, which is relatively large. However, it is not possible to expect the mathematical model to issue values with more precision than the experimental accuracy. Considering the

TABLE II Experimental values of flexural strength at room temperature and at 1200 °C

	TiB_2 (mol %)	TiC	SiC	σ_f 1200 °C (MPa)	σ_f *RT* (MPa)	$\Delta\sigma_f$ (%)
14	67	16.5	16.5	461 ± 39	966 ± 40	52.3
15	16.5	67	16.5	358 ± 25	929 ± 151	61.5
16	16.5	16.5	67	572	775 ± 29	26.2
18	20	55	25	456 ± 51	1216 ± 95	62.5

TABLE III Experimental values of fracture toughness and their differences with polynomial models of first and second degrees

	TiB_2 (mol %)	TiC	SiC	Fracture toughness (MPa $m^{1/2}$)	Differences with polynomial models of degree 1st	2nd
1	100	0	0	5.0 ± 0.8	− 0.8	0.1
2	0	100	0	4.4 ± 0.6	1.3	0
3	0	0	100	2.9 ± 0.5	1.7	0.1
4	50	50	0	5.2 ± 0.4	0.5	0.2
5	50	0	50	5.1 ± 0.8	0.0	0.3
6	0	50	50	6.3 ± 0.9	− 1.2	0.2
7	33	33	33	5.9 ± 0.8	− 0.6	0.4
14	67	16.5	16.5	6.4 ± 0.5	− 0.9	− 0.6
15	16.5	67	16.5	6.2 ± 0.4	− 0.7	− 0.2
16	16.5	16.5	67	5.9 ± 0.5	− 1.0	− 0.4
					test points	
8	67	33	0	4.9 ± 0.4	0.8	0.6
9	33	67	0	5.2 ± 0.5	0.5	0.0
10	67	0	33	6.3 ± 0.4	− 0.9	− 0.7
11	33	0	67	4.2 ± 0.2	0.8	0.7
12	0	67	33	6.4 ± 0.2	− 1.1	0.0
13	0	33	67	5.6 ± 0.3	− 0.7	0.3
17	32	55	13	6.7 ± 0.5	− 1.1	− 0.7
18	20	55	25	6.4 ± 0.7	− 1.1	− 0.1

confidence it is possible to have in fracture toughness measurements using Vickers indentation technique, as well as their standard deviation, the accuracy of the predicted values is within $\pm$ 1 MPa $m^{1/2}$.

The isofracture toughness curves plot is given in Fig. 7. It is particularly interesting to study the toughness evolution at the experimental field boundaries. On the TiB_2–TiC axis, major reinforcement effects are not expected since the CTE of both materials are similar. However, their good cohesion allows for a steady stage of about 5 MPa $m^{1/2}$ to be reached (composites No. 4, 8, 9).

On the TiB_2–SiC axis, the situation is more differentiated. The large CTE mismatch allows for reinforcement effects to be expected, however, the lack of cohesion between both materials will be a limiting factor. On the TiB_2 side, the bonding problem has no importance since the SiC discrete particles are put under compression by the surrounding TiB_2 matrix. This may cause microcracking and, hence, increase the fracture toughness, i.e. 6.4 MPa $m^{1/2}$ for composite No. 10. On the SiC side, the large TiB_2 CTE causes this second phase to shrink from the SiC matrix, since there are only weak bonds between these phases, decohesion of the TiB_2 particles may occur. This explains the moderate fracture toughness of composite No. 11, i.e. 4.2 MPa $m^{1/2}$.

On the TiC–SiC axis, both the large CTE mismatch and the strong bonds developed between the materials are favourable in terms of reinforcement effects. On the TiC side, microcracking may occur in the TiC matrix around the SiC particles, with its propitious consequences already described, i.e. 6.4 MPa $m^{1/2}$ for composite No. 12. On the SiC side, the TiC discrete particles will again tend to shrink away from the SiC matrix. However, this time, the strong bonds developed between the materials, will avoid decohesion and, furthermore, will cause the SiC matrix to come into compression. This is an efficient toughening mechanism, i.e. 5.6 MPa $m^{1/2}$ for composite No. 13. The steady stage of the fracture toughness values for the three phase composites (No. 7, 14, 15, 16) around 6 MPa $m^{1/2}$ seems to indicate, that whatever the toughening mechanisms are, their benefit is similar. For composite 15, some crack branching is observed (Fig. 8b), and for composite 14 and 16, crack deflection and crack pinning (Fig. 8a and c) are the main mechanisms.

4.4. Critical flaw size

Since the bend strength as well as the fracture toughness are known, it is interesting to compute the critical

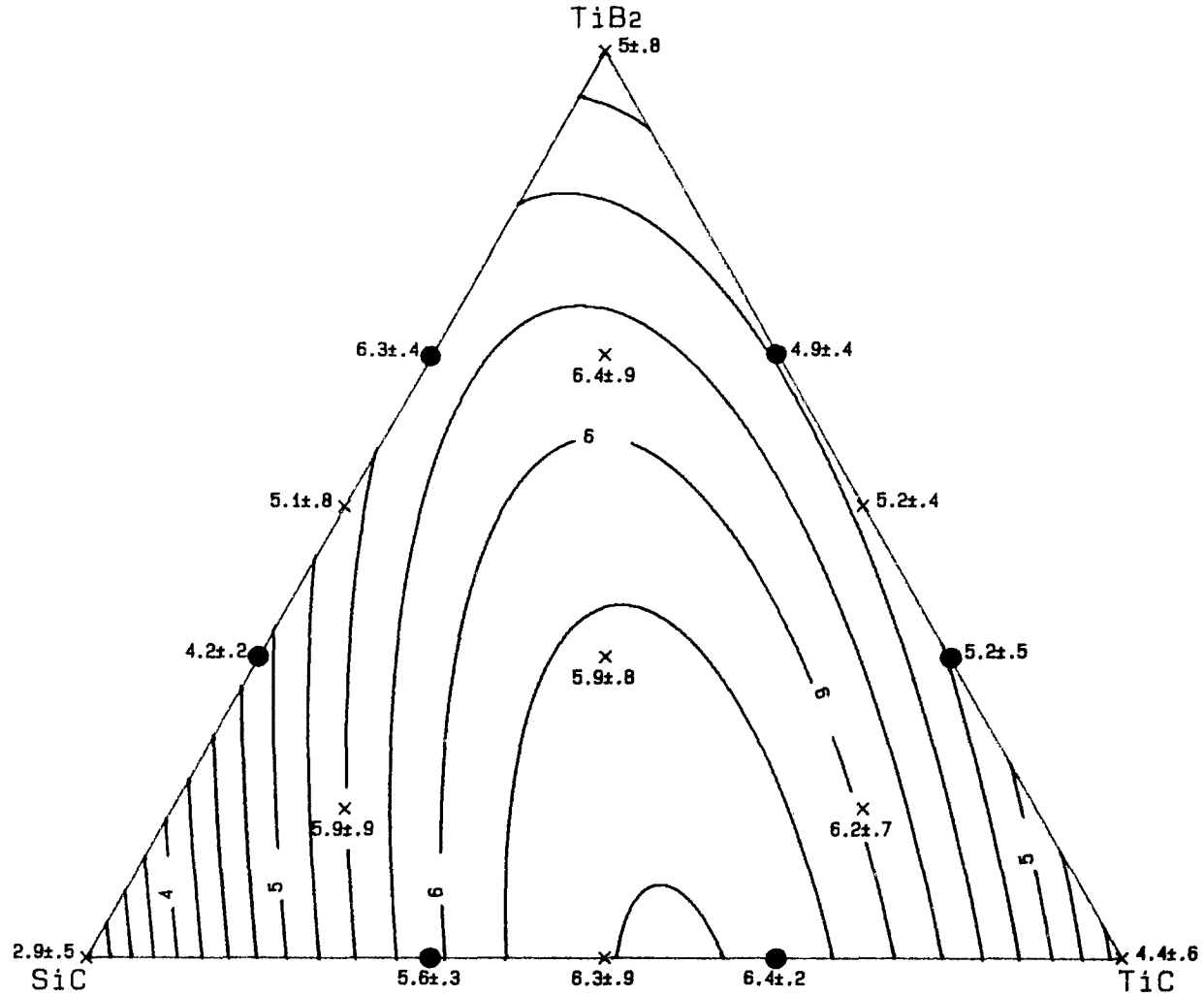

Figure 7 Isofracture toughness curves plotted using a second order polynomial model. The incrementation step between two curves is 0.25 MPa $m^{1/2}$. The black points are test points.

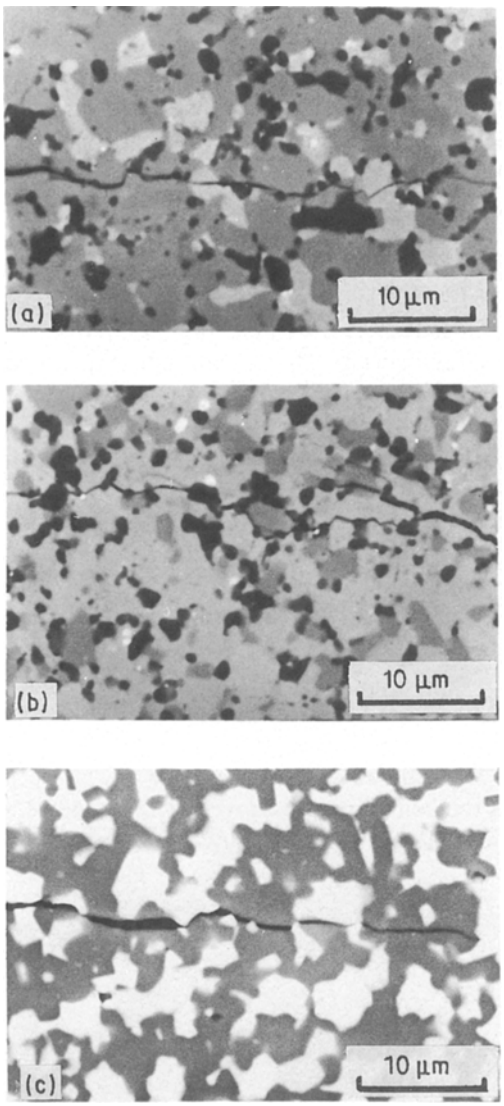

Figure 8 Cracks morphology in three phase composites: (a) 67% TiB_2 (grey)–16.5% TiC (white)–16.5% SiC (black); (b) 16.5% TiB_2 – 67% TiC–16.5% SiC; and (c) 16.5% TiB_2–16.5% TiC–67% SiC.

flaw size using Griffith relation

$$a = 0.268\left(\frac{K_{1c}}{\sigma_f}\right)^2 \quad (3)$$

Its standard deviation arises from strength's and toughness' one. Table IV lists the critical flaw sizes and their differences with several polynomial models. Their values range from 6 μm on the TiB_2–TiC axis to 18 μm on the TiB_2–SiC axis. A third order polynomial model is necessary to fit the data within the computed standard deviation.

$$\begin{aligned} Y = {} & 8.19X_1 + 17.02X_2 + 8.71X_3 \\ & - 24.92X_1X_2 + 23.44X_1X_3 - 4.38X_2X_3 \\ & + 19.2X_1X_2(X_1 - X_2) - 4.89X_1X_3 \\ & \times (X_1 - X_3) - 32.2X_2X_3(X_2 - X_3) \\ & - 20.36X_1X_2X_3 \end{aligned} \quad (4)$$

where Y is the critical flaw size μm and X_i the molar fraction of i, with 1 : TiB_2, 2 : TiC, 3 : SiC.

The evolution of the critical flaw size in the ternary system is shown in Fig. 9. For the binary and ternary composites, to high modulus of rupture correspond small critical flaw sizes and conversely. This is an expected trend since the variation of fracture toughness in this area is rather low.

4.5. Hardness

The Vickers hardness (1 kg load) of the different composites are listed in Table V. The hardness values range form 17.5 GPa for pure TiB_2 to 32.3 GPa for pure SiC. In Table V, the differences Δ between the experimental hardness and the values computed with polynomial models of different orders are also reported.

With the linear model, the Δ values ranges from 0 to 3.1 GPa. Since the confidence it is possible to have in

TABLE IV Computed values of critical flaw size and their differences with polynomial models of first, second and cubic degrees

	TiB_2 (mol %)	TiC	SiC	Critical flaw size (μm)	Differences with polynomial models of degree 1st	2nd	3rd
1	100	0	0	8.5 ± 3.2	− 0.1	0.1	− 0.3
2	0	100	0	17.2 ± 8.0	− 5.8	− 1.2	− 0.2
3	0	0	100	9.0 ± 4.9	3.9	0.6	− 0.3
4	50	50	0	8.0 ± 2.9	1.8	− 1.7	− 1.6
5	50	0	50	17.7 ± 8.0	− 7.0	− 3.5	− 3.4
6	0	50	50	13.0 ± 5.7	− 0.8	− 1.3	− 1.2
7	33	33	33	9.9 ± 4.3	1.0	0.6	0.0
8	67	33	0	6.1 ± 2.6	3.3	− 0.4	0.9
9	33	67	0	6.2 ± 3.0	4.2	2.0	0.9
10	67	0	33	11.3 ± 3.2	− 1.4	2.1	1.9
11	33	0	67	12.2 ± 1.7	− 0.8	1.5	1.9
12	0	67	33	10.2 ± 2.1	1.6	2.7	0.7
13	0	33	67	12.2 ± 5.1	0.2	− 1.4	0.7
					test points		
14	67.0	16.5	16.5	11.4 ± 4.3	− 1.8	− 2.0	− 1.5
15	16.5	67.0	16.5	8.9 ± 1.6	2.2	2.2	− 0.6
16	16.5	16.5	67.0	18.2 ± 5.5	− 6.3	− 6.6	− 5.1
18	20.0	55.0	25.0	9.5 ± 4.0	1.6	1.2	− 1.1

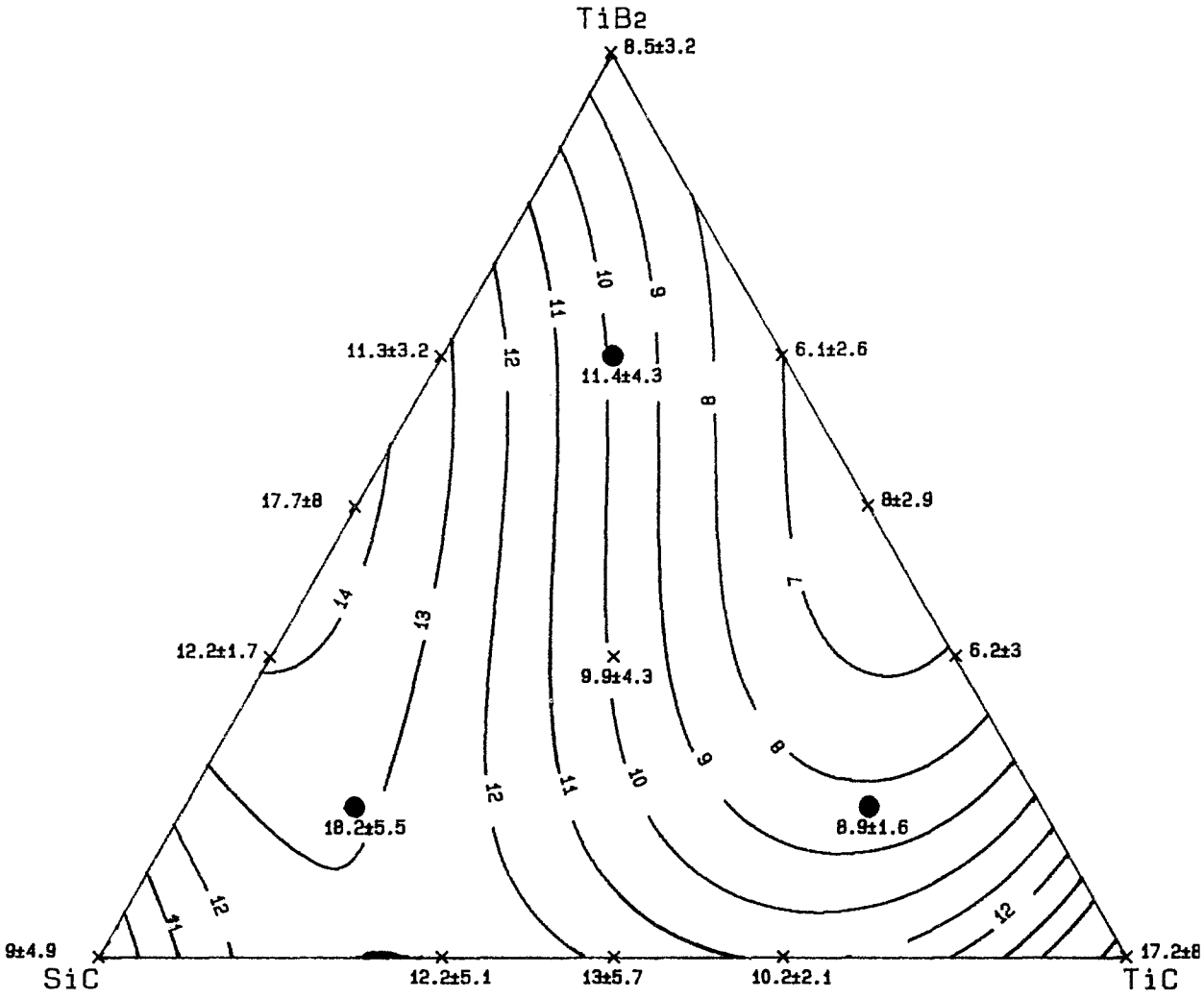

Figure 9 Isocritical flaw sizes curves plotted using a third order polynomial model. The incrementation step between two curves is 1 μm. The black points are test points.

TABLE V Experimental hardness values and their differences with polynomial models of first, second and third degrees

	TiB_2 (mol %)	TiC	SiC	Experimental hardness (GPa)	Differences with polynomial models of degree 1st	2nd	3rd
1	100	0	0	17.5 ± 0.6	3.1	0.5	0.0
2	0	100	0	26.7 ± 1.9	0.0	− 0.1	− 0.1
3	0	0	100	32.3 ± 1.5	0.0	0.0	0.0
4	50	50	0	25.3 ± 1.1	− 1.7	− 0.6	− 0.4
5	50	0	50	28.1 ± 2.6	− 1.6	− 0.6	− 0.4
6	0	50	50	29.0 ± 2.4	0.5	− 0.6	− 0.4
7	33	33	33	26.3 ± 0.7	0.3	1.0	0.0
8	67	33	0	23.9 ± 2.0	− 1.3	− 0.9	0.2
9	33	67	0	24.8 ± 1.4	− 0.1	1.0	0.2
10	67	0	33	24.9 ± 2.1	− 0.4	0.0	0.2
11	33	0	67	29.5 ± 2.5	− 1.1	0.1	0.2
12	0	67	33	27.9 ± 2.2	0.7	− 0.3	0.2
13	0	33	67	29.0 ± 2.9	1.5	0.5	0.2
					test points		
14	67.0	16.5	16.5	25.2 ± 1.1	− 1.7	− 1.4	− 1.1
15	16.5	67.0	16.5	26.4 ± 1.4	0.2	0.6	− 0.3
16	16.5	16.5	67.0	28.8 ± 1.7	0.7	1.0	0.2
18	20.0	55.0	25.0	26.6 ± 1.0	0.3	0.7	− 0.4

hardness measurements is estimated to be ± 2 GPa, this model is discarded. With the quadratic model, the Δ values are smaller than 1 GPa for the points used for the polynomial fitting and Δ reaches 1.4 GPa for the test points. Considering the hardness measurements precision, this model is in good agreement with the experimental values. The cubic model matches the experimental points even better, i.e. $\Delta_{fitting} < 0.4$ GPa

and $\Delta_{test} < 1$ GPa. However, there is no point in having a polynomial model predicting hardness values with a better precision than the physical measurements. And since we are looking for an empirical model as simple as possible, we conclude that the quadratic polynomial model (Equation 5) is sufficient to satisfactorily describe and predict (Fig. 10) the evolution of the hardness in the ternary system TiB_2–TiC–SiC.

$$Y = 17.95X_1 + 26.6X_2 + 32.2X_3 + 9.7X_1X_2 + 9.8X_1X_3 - 4X_2X_3 \quad (5)$$

where Y is the computed hardness and X_i the molar fraction of i, with 1 : TiB_2, 2 : TiC, 3 : SiC.

4.6. Coefficient of thermal expansion

The coefficients of thermal expansion, CTE, were measured between 20 and 1200 °C under argon. Their values range from $5.1 \times 10^{-6} K^{-1}$ for SiC to $8.4 \times 10^{-6} K^{-1}$ for TiC (Table VI). The precision of the measure is $\approx 0.1 \times 10^{-6} K^{-1}$. It is, therefore, concluded that a linear model (Equation 6) is satisfactory to describe (Fig. 11) the CTE evolution in the complete ternary system.

$$Y = 7.75X_1 + 8.31X_2 + 5.11X_3 \quad (6)$$

where Y is the computed CTE and X_i the molar fraction of i, with 1 : TiB_2, 2 : TiC, 3 : SiC.

Turner [17] developed a model to compute the CTE of composite materials. Assuming that no cracks develop, that the contraction of each grain is the same as the overall contraction, and that all microstresses are purely hydrostatic tension and compression, Relation 7 is obtained. The values computed with this relation are in good agreement with both the experimental data and the predicted values with the 1st order polynomial model.

$$\alpha_c = \frac{(\alpha_1 K_1 F_1/\rho_1) + (\alpha_2 K_2 F_2/\rho_2) + (\alpha_3 K_3 F_3/\rho_3)}{(K_1 F_1/\rho_1) + (K_2 F_2/\rho_2) + (K_3 F_3/\rho_3)} \quad (7)$$

where α_c is the overall CTE (K^{-1}), α_i the CTE of phase i (K^{-1}), K_i the bulk modulus (Pa), F_i the weight fraction, and ρ_i the phase density (g cm^{-3}).

4.7. Electrical resistivity

The electrical resistivity ρ of pure TiB_2 given in Table VII, is rather low, i.e. 13 $\mu\Omega$ cm; it is equivalent to that

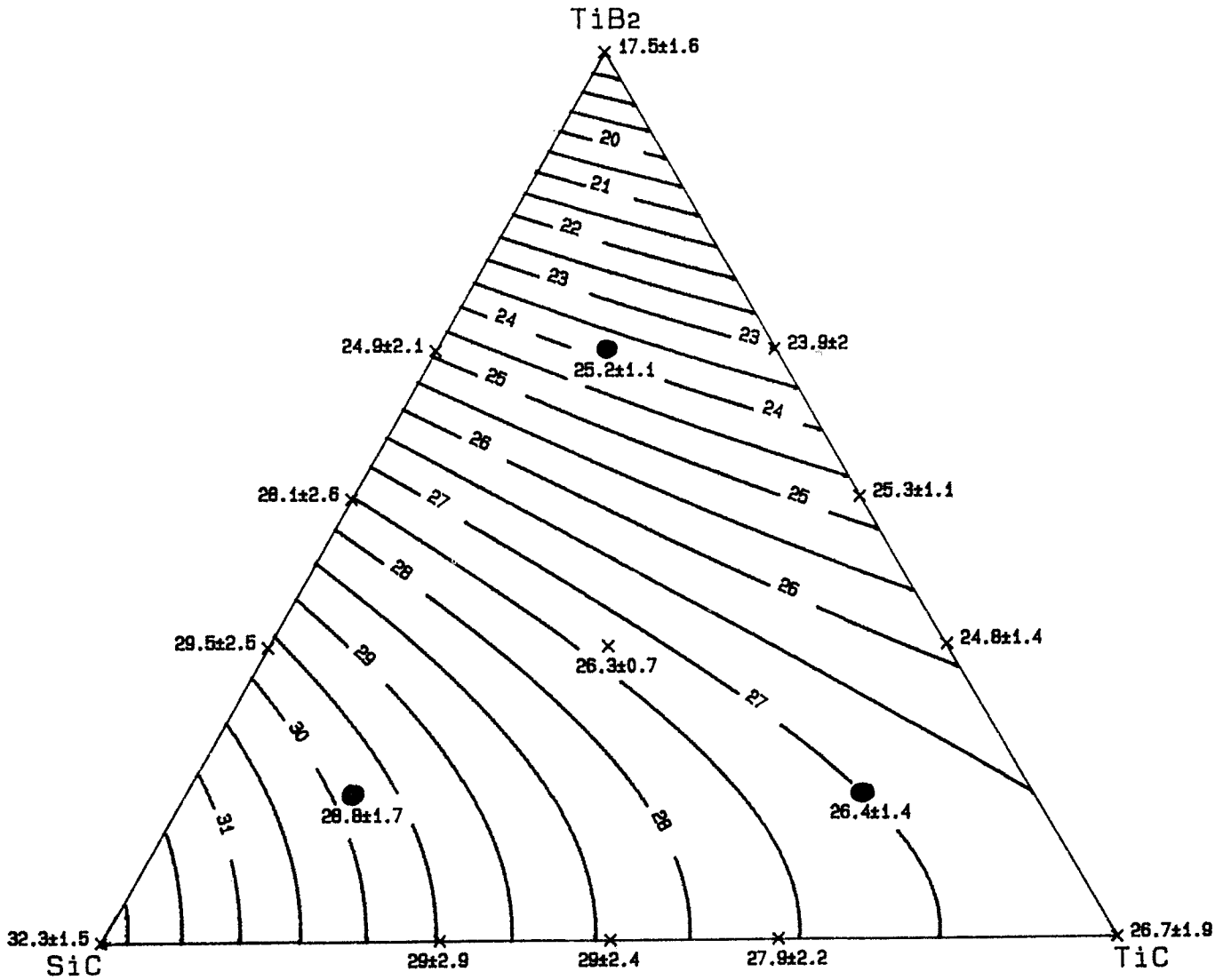

Figure 10 Isohardness curves plotted using a second order polynomial model. The incrementation step between two curves is 0.5 GPa. The black points are test points.

TABLE VI Experimental coefficient of thermal expansion values and values computed with a first degree polynomial and Turner models

	TiB_2 (mol %)	TiC	SiC	Coefficient of thermal expansion ($10^{-6}K^{-1}$)	Computed with a 1st degree model	Turner model
1	100	0	0	7.8	7.8	–
2	0	100	0	8.4	8.3	–
3	0	0	100	5.1	5.1	–
4	50	50	0	7.8	8.0	8.1
5	50	0	50	6.4	6.4	6.5
6	0	50	50	6.6	6.7	6.8
7	33	33	33	7.3	7.1	7.1
					test points	
14	67.0	16.5	16.5	7.5	7.4	7.5
15	16.5	67.0	16.5	7.7	7.7	7.8
16	16.5	16.5	67.0	6.2	6.1	6.1
18	20.0	55.0	25.0	7.4	7.4	7.5

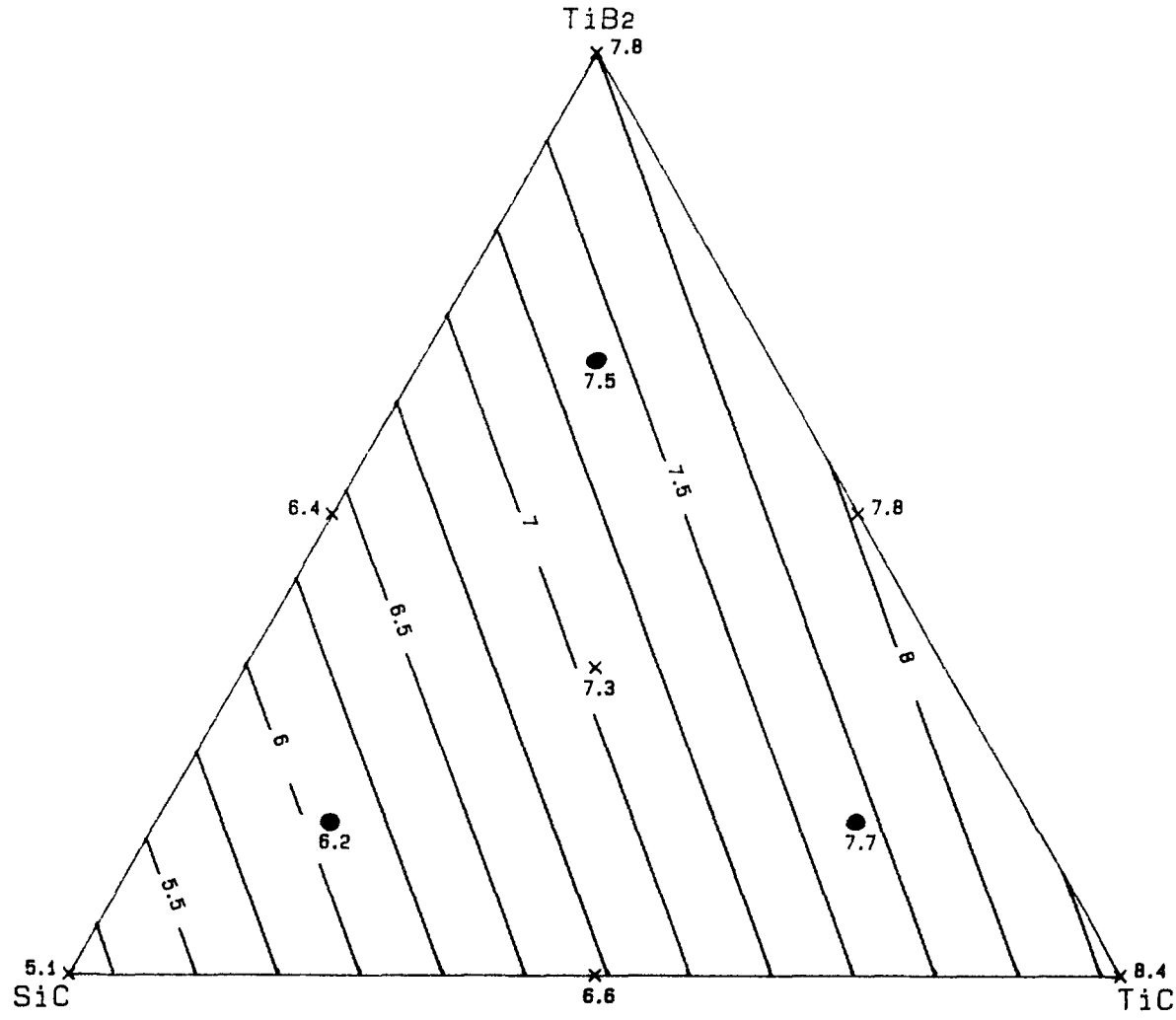

Figure 11 Isocoefficient of thermal expansion curves plotted using a linear model. The incrementation step between two curves is $0.25 \times 10^{-6} K^{-1}$. The black points are test points.

of steel and tin. TiC resistivity is somewhat higher, i.e. 64 μΩ cm. This corresponds to constantan or mercury. Although SiC is a semi-conductor, processed under the present conditions, it is non-conductor, i.e. 10^{13} μΩ cm.

As can be seen, the ρ values of pure SiC is about 10^{10} times larger than the highest value measured for the other composites (point 13). It is impossible for a polynomial model to accommodate such a huge difference. By taking the logarithm of the resistivity, the difference factor is reduced to 5, i.e. form 13 for point 3 to 2.8 for point 13. It may be possible for a polynom to fit these new data, however, its degree will have to be superior or equal to 4. In this study we

TABLE VII Experimental electrical resistivity values, their logarithms, their differences with a polynomial model of third degree, and values computed with Landauer model

	TiB_2 (mol %)	TiC	SiC	Experiment resistivity ($\mu\Omega$ cm)	Logarithm of resistivity exp.	calc.	Resistivity comp. ($\mu\Omega$ cm)	diff.	Landauer model
1	100	0	0	13.1 ± 0.1	1.117	1.118	13.2	0.1	–
2	0	100	0	64.0 ± 1.3	1.806	1.809	64.4	0.4	–
3	0	0	100	1 E 13	–	–	–	–	–
4	50	50	0	21.1 ± 0.1	1.324	1.351	22.4	1.3	23
5	50	0	50	46.1 ± 0.3	1.664	1.665	46.2	0.1	39
6	0	50	50	220 ± 1.0	2.342	2.359	228.6	8.6	267
7	33	33	33	50.6 ± 1.0	1.704	1.704	50.6	0	69
8	67	33	0	18.7 ± 0.2	1.272	1.257	18.1	− 0.6	18
9	33	67	0	30.6 ± 0.3	1.486	1.471	29.6	− 1	31
10	67	0	33	26.6 ± 0.9	1.425	1.425	26.6	0	22
11	33	0	67	127 ± 1.6	2.103	2.103	126.9	0	–
12	0	67	33	114 ± 1.0	2.057	2.048	111.7	− 2.2	129
13	0	33	67	632 ± 6.0	2.801	2.792	619.4	− 12.6	–
					test points				
14	67	16.5	16.5	21.2 ± 0.1	1.326	1.357	22.8	1.6	20
15	16.5	67.0	16.5	49.7 ± 0.7	1.696	1.699	50.0	0.3	56
16	16.5	16.5	67.0	313 ± 2.6	2.496	2.455	285.1	− 2.8	–
17	32	55.0	13.0	36.9 ± 0.2	1.567	1.549	35.4	− 1.5	37
18	20	55.0	25.0	57.4 ± 0.6	1.759	1.741	55.0	− 2.4	60

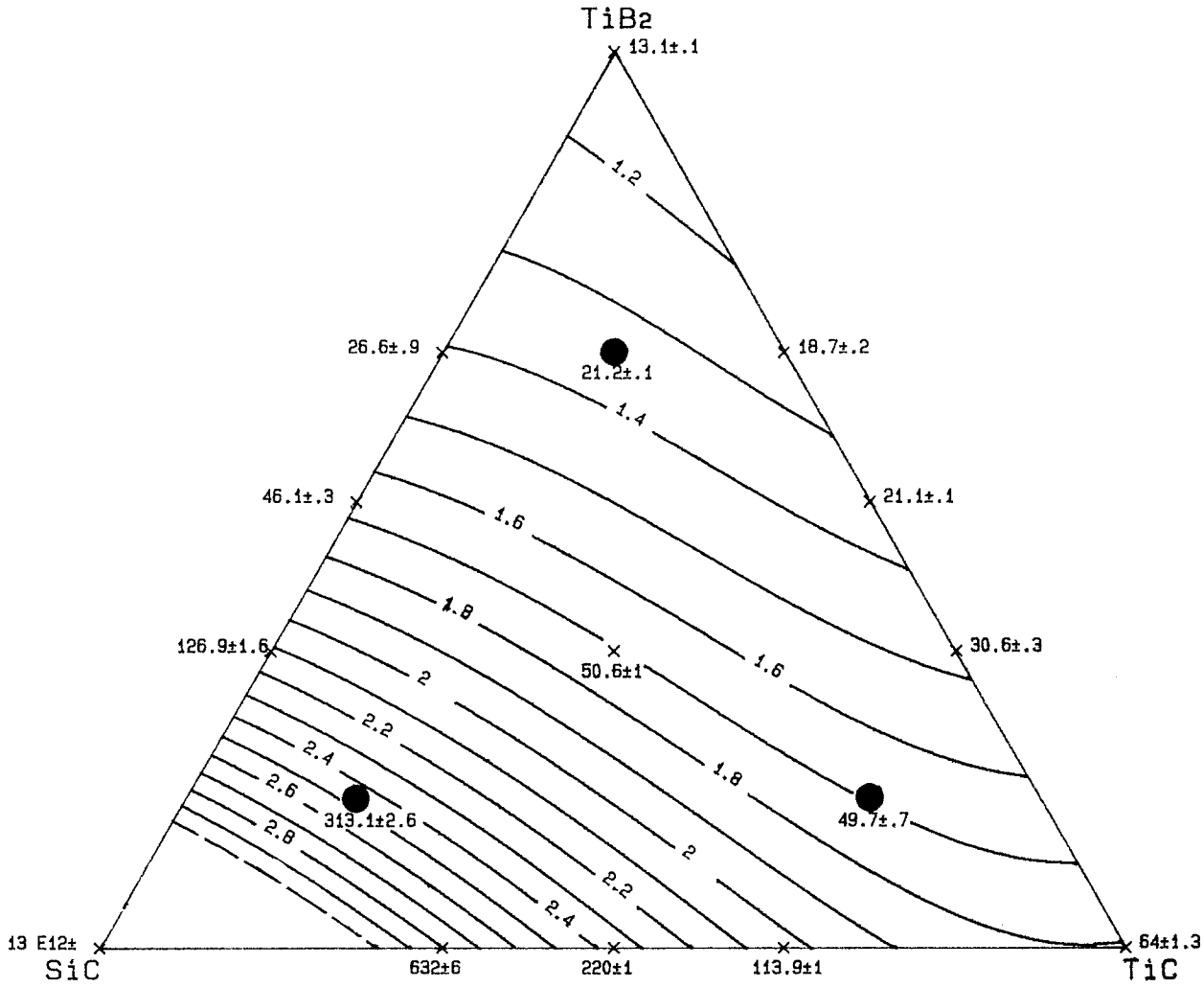

Figure 12 Isocurves of the logarithm of the electrical resistivity plotted using a third order polynomial model. The incrementation step between two curves is 0.1 log $\mu\Omega$ cm. The black points are test points.

decided to limit the polynomial models to the third order to stay within the limit of 20 different compositions and since our only pretension is to find an empirical model describing the evolution of the electrical resistivity, we tried to find a value for the logarithm of SiC resistivity that would allow for an accurate second or third order polynomial fitting on every other point. A third order polynomial model (Equation 8) with a value log $\rho_{SiC} = 4$ is perfectly satisfactory.

$$\begin{aligned} Y = {} & 1.119 X_1 + 1.809 X_2 + 4.001 X_3 \\ & - 0.45 X_1 X_2 - 3.581 X_1 X_3 - 2.184 X_2 X_3 \\ & + 0.108 X_1 X_2 (X_1 - X_2) + 1.902 X_1 X_3 \\ & \times (X_1 - X_3) - 0.089 X_2 X_3 (X_2 - X_3) \\ & + 2.297 X_1 X_2 X_3 \end{aligned} \quad (8)$$

where Y is the logarithm of the electrical resistivity and X_i the molar fraction of i, with 1: TiB_2, 2: TiC, 3: SiC.

The differences Δ between the computed and the experimental resistivity are given in Table VII. They are very satisfactory since $\Delta_{fitting} < 12.6\ \mu\Omega\,cm$ and $\Delta_{test} < 2.8\ \mu\Omega\,cm$. The isoresistivity curves are shown in Fig. 12. Obviously, this model with the logarithm of the resistivity is only valid up to the last real measured point (point 13). Therefore, no prediction can be made in the SiC corner.

Models to calculate the conductivity ($\sigma = 1/\rho$) of composite bodies were developed by different authors [18]. The theory of effective medium (Landauer [19]) assumes that every dipersed particle of conductivity σ_1 is located in a medium of mean conductivity σ_m. Therefore, the mean electrical field is not particularly disturbed by the particle and its value is equal to the applied field. The mean conductivity can then be calculated with Relation 9.

$$\frac{\sigma_1 - \sigma_m}{\sigma_1 - 2\sigma_m} X_1 + \frac{\sigma_2 - \sigma_m}{\sigma_2 - 2\sigma_m} X_2 + \frac{\sigma_3 - \sigma_m}{\sigma_3 - 2\sigma_m} X_3 = 0 \quad (9)$$

where σ_m is the composite conductivity ($\Omega^{-1}\,cm^{-1}$), σ_i the conductivity of constituent i, and X_i the volumic fraction of constituent i.

In our case, one constituent being insulating ($\sigma_{SiC} = 0$), Relation 9 simplifies into a second order polynom. However, the validity of this model is limited to composites containing no more than 50% SiC. The agreement between values issued from experiments and from the Landauer model is satisfactory (Table VII).

5. Conclusions*

The use of a methodology of research using optimal design allows the number of samples to be drastically reduced, i.e. 16 compositions, necessary to describe and predict the evolution of mechanical and electrical properties, i.e. modulus of rupture σ_f, fracture toughness K_{1c}, critical flaw size a_c, hardness Hv, coefficient of thermal expansion α and electrical resistivity ρ over the complete ternary system TiB_2–TiC–SiC. Third order polynomial models are perfectly satisfactory to describe the flexural strength, the critical flaw size and the electrical resistivity; for the fracture toughness and the hardness quadratic models are already sufficient, and for the CTE, a linear model is satisfactory.

The mathematical model predicts a maximum bend strength for the composition 32 mol % TiB_2–55 mol % TiC–13 mol % SiC, i.e. 1083, in excellent agreement with the experimental measure, i.e. 1073 ± 131 MPa. The location of this maximum can be explained by the fact that strong bonds are able to develop between TiC and TiB_2 and between TiC and SiC particles. Therefore every TiB_2 and SiC reinforcement particles are firmly bonded to the TiC matrix. A fracture toughness of $\approx 6\ MPa\,m^{1/2}$ is found for every three phase composites. The fracture toughness evolution is explained by the coefficient of thermal expansion mismatch between SiC on one side and TiC, TiB_2 on the other, and by their cohesion differences. The main toughening mechanisms observed are crack deflection and crack pinning.

We may imagine the use of such a composite as structural ceramics (for dies, cutting tools, etc.), crucibles, electrodes for molten metals or resistors. In function of this latter application, one composition with good characteristics is selected. The elaboration process of this composite is optimized, its pressureless sinterability assessed and its mechanical properties studied in deeper details, i.e. thermal shock resistance, high temperature bend strength, etc. This is reported in Part II.

References

1. R. E. MURASHKO and V. N. SUMAROKOV *et al.*, *Poroshkovaya Metallurgya (Eng.)* **4** (1978) 85.
2. W. A. ZDANIEWSKI, *Amer. Ceram. Soc. Bull.* **65** (1986) 1408.
3. C. H. McMURTRY and W. D. G. BOECKER *et al.*, *Amer. Ceram. Soc. Bull.* **66** (1987) 325.
4. M. A. JANNEY, *Amer. Ceram. Soc. Bull.* **66** (1987) 322.
5. L. N. DOAN, "Gefügeverstärkung von SiC-Keramiken", Dissertation (Max-Planck Institut, Stuttgart (RFA) 1988).
6. G. C. WEI and P. F. BECHER, *J. Amer. Ceram. Soc.* **67** (1984) 571.
7. I. HAHN, "Hochtemperator und Thermoschock-eigenschaften von gefügeverstärktem Siliciumkarbid", Diplomarbeit (Max-Planck Institut, Stuttgart (RFA) 1989).
8. G. DAS, K. S. MAZDIYASNI and H. A. LIPSITT, *J. Am. Ceram. Soc.* **65** (1982) 104.
9. E. FARGIN and M. SERGENT *et al.*, *Bio-Sciences*, **4** (1985) 77.
10. R. PHAN-TAN-LUU, D. MATHIEU and D. FENEUILLE, Méthodologie de la recherche expérimentale, Fascicules de cours, L.P.R.A.I. (Université d'Aix-Marseille, 1983).
11. M. SERGENT, D. MATHIEU and R. PHAN-TAN-LUU, *R.F. OE.* **98**, 36.
12. D. MATHIEU and R. PHAN-TAN-LUU, Logiciel NEMROD, L.P.R.A.I. (Université d'Aix-Marseille, 1988).
13. C. BRODHAG, M. BOUCHACOURT and F. THEVENOT, *Silicates Industriels* **4-5**, 91.

* Note: the present work and its conclusions are based, in part, on doctoral research of one of the present authors (F. deM.) [20].

14. C. BRODHAG, Thesis N° 83-27 (Limoges, 1983).
15. S. S. ORDON'YAN, V. I. UNROD and A. I. AVGUSTINIK, *Poroshkovaya Metallurgya (Eng.)* **9** (1975) 40.
16. D. L. JIANG, J. H. WANG, Y. L. LI and L. T. MA, *Materials Science and Engineering* **A109**, 401.
17. TURNER, *J. Res. NBS* (1946), 37,239.
18. J. P. CLERC, G. GIRAUD, J. ROUSSENQ, R. BLANC, J. P. CARTON, E. GUYON, H. OTTAVIAND and D. STAUFFER, "La percolation", ed. Annales de Physique (Masson, Paris, 1983) p. 1.
19. R. LANDAUER, *J. Appl. Phys.* **23** (1952) 779.
20. F. de MESTRAL, Thesis N° 41 TD (Ecole Nationale Supérieure des Mines, St Etienne, France, 1990).

Received 11 June
and accepted 26 June 1990